Supplementary Information (SI) for Dalton Transactions.
This journal is © The Royal Society of Chemistry 2025

Expanding silver fluorooxoborate crystal chemistry: $Ag_2B_5O_8F$ with 3D double interpenetrating frameworks and $Ag_3B_5O_8F_2$ with 2D layers

Sergey Volkov, Xia Yang[#], Vadim Kireev, Alexander Banaru, Shujuan Han*, Alevtina Gosteva, Maxim Arsent'ev, Dmitri Charkin, Alexey Povolotskiy, Yevgeny Savchenko, Maria Krzhizhanovskaya, Stepan Vorobiev, Yulia Vaitieva, Sergey Aksenov, Fangfang Zhang*

1. Reagents

$AgNO_3$ (Lenreactiv, Russia, 99.0 %), $AgBF_4$ (LEAPChem, China, 99.0 %), Ag_2O (Macklin, China, 99.9 %), phase identification of the prepared samples was carried out using a Rigaku Miniflex II (30 kV/10 mA) diffractometer utilizing Cu Kα radiation ($\lambda_{K\alpha1}$ = 1.540598 Å, $\lambda_{K\alpha2}$ = 1.54433 Å).

2. Single crystal preparation and the synthesis of compounds

Single crystals of $Ag_2B_5O_8F$ (**1**) and $Ag_3B_5O_8F_2$ (**2**) were obtained by the sealed ampoule synthesis method. Crystals **1** were obtained by mixing of $AgBF_4$ (0.3711 g, 1.906 mmol) and calcinated B_2O_3 (0.2654 g, 3.812 mmol). The mixture was thoroughly ground in a glove box under an nitrogen atmosphere, then placed in a vacuum-sealed quartz ampoule. The use of a glove box and nitrogen atmosphere is necessary because $AgBF_4$ is strongly sensitive to atmospheric moisture. We tried to perform the synthesis in an open atmosphere, but it turned out to be impossible. A lot of liquid appears in the sample after 1–2 minutes of grinding in an agate mortar in an open atmosphere, as a result of which the sample deliquesces and is no longer dry. The sample was heated at a rate of 30 °C h^{-1} to 200 °C, held at this temperature for 24 h, and then heated at a rate of 30 °C h^{-1} to 300 °C, held for 48 h, after which it was heated to 400 °C in 12 h and held at this temperature for 72 h. Crystals of **1** were selected from the resulting sample.

Crystals **2** were obtained by equimolar mixing of $AgBF_4$ (0.2400 g, 1.233 mmol), calcinated Ag_2O (0.2857 g, 1.233 mmol) and B_2O_3 (0.0858 g, 1.233 mmol), within a glove box under a nitrogen atmosphere. The mixture was placed in a vacuum-sealed quartz ampoule, which was subjected to a temperature treatment similar to that used for **1**. Crystals of **2** were selected from the sample.

To characterize the properties, we synthesized polycrystalline samples of these two compounds. To obtain **1**, we mixed $AgBF_4$ (0.4000 g, 2.055 mmol) and B_2O_3 (0.1907 g, 2.740 mmol) in a stoichiometric ratio, and the mixture was placed in an evacuated quartz ampoule, heated to 400 °C for 4 days, maintained at this temperature for 67 h, and then cooled to 100 °C for 2 days. The resulting sample consisted of 91 wt % of **1**, along with 6 wt % of α′-$Ag_2B_8O_{13}$ and 3 wt % of metallic Ag (Figure S1a).

To obtain polycrystalline sample of **2**, $AgBF_4$ (0.3741 g, 1.922 mmol), Ag_2O (0.2227 g, 0.961 mmol) and B_2O_3 (0.0669 g, 0.961 mmol) were thoroughly mixed within a glove box under a nitrogen atmosphere, and the mixture was placed in a sealed evacuated quartz ampoule. The sample was then heated at a rate of 30 °C h^{-1} to 200 °C, held at this temperature for 24 h, then also heated at a rate of 30 °C h^{-1} to 300 °C, held for 48 h, after which it was heated to 400 °C in 12 h and held at this temperature for 72 h. The resulting sample was virtually homogeneous **2**. The intensity of one unidentified peak on the X-ray diffraction pattern at 25.97 and 27.93 ° did not exceed 4% of the strongest peak (Figure S1b).

It should be noted that numerous attempts to obtain **2** from a mixture of $AgBF_4$ and B_2O_3 according to the reaction $9AgBF_4 + 8B_2O_3 = 3Ag_3B_5O_8F_2 + 10BF_3\uparrow$ were unsuccessful. The presence of silver oxide appears to be a necessary condition, as indicated by the reaction: $(9b–13a)AgBF_4+8aAg_2O+8bB_2O_3=(a+3b)Ag_3B_5O_8F_2+(10b–18a)BF_3\uparrow$, where $0<a\leq0.3125$, $0.5625\leq b<1$.

3. Structure determination

Single crystals of **1** (0.04 × 0.08 × 0.12 mm^3) and **2** (0.07 × 0.09 × 0.13 mm^3) were selected under polarized light using an optical microscope and subsequently attached to a glass fiber using epoxy glue. Lorentz and polarization corrections were applied. The experimental data were collected on a Rigaku XtaLAB Synergy-S four-circle diffractometer. The absorption correction based on the crystal shape was performed.[2] An isotropic extinction correction did not improve the refinement for both crystals. The observed Laue symmetry and systematic absences indicated the *Pbca* and $P2_1/n$ space groups for **1** and **2**, respectively. The structures were solved using a charge-flipping method[3] implemented in JANA2020.[4] Data visualization was performed by the Vesta[5] and Atoms6.1[6] software. During the structure determination and refinement, 2 Ag, 5 B, 8 O, and 1 F were localized for **1,** while 3 Ag, 8 O, 5 B, and 2 F were localized for **2**. The final

models included anisotropic displacement parameters for all atoms. The main features of the X-ray diffraction experiment and structure refinement are summarized in Table S1. Final atomic positional and displacement parameters, as well as selected bond lengths and angles are given in Tables S2−S7. The bond valence sums for the Ag, B, O, and F atoms were calculated and are listed in Tables S2 and S4 confirming the expected oxidation states of +1, +3, –2, and –1, respectively. CCDC 2394280, 2394281 contain the supplementary crystallographic data for this paper. These data are provided free of charge by The Cambridge Crystallographic Data Centre.

4. EDX studies

Energy-dispersive X-ray spectroscopy (EDX) was conducted on a Zeiss EVO-25 scanning electron microscope (SEM) equipped with an Oxford Instruments Ultum-Max 100 Energy Dispersive Spectrometer. The electron-beam was accelerated at a voltage of 20 kV with a current of 2 nA, utilizing a defocused beam with a spot size up to 4 μm. The X-ray acquisition time was set to 100 s. The chemical composition was measured on different spots on several crystals and eventually averaged. The final composition was normalized to 100 %. EDX analysis reveals Ag:B:O:F molar ratios of approximately 2.0:5.0:8.2:0.8 and 3.0:4.6:8.0:1.5, which are close to the expected ratios of 2:5:8:1 for **1** and 3:5:8:2 for **2** (Figure S2). In addition, according to the general rules for inductively coupled plasma optical emission spectrometry JYT0567-2020, we have measured the amount of B in $Ag_2B_5O_8F$ using agilent 5900 SVDV ICP-OES. The amount of B in $Ag_2B_5O_8F$ is 12.9%, which is consistent with the theoretical value.

5. Variable-temperature X-ray powder diffraction

The thermal behavior of **2** was studied by high-temperature X-ray powder diffraction using a Rigaku Ultima IV diffractometer (Cu Kα radiation, 40 kV/30 mA, Bragg-Brentano geometry, PSD D-Tex Ultra) with 20 °C temperature increments in the range 40–400 °C (Rigaku R-300 high-temperature attachment). The unit cell parameters were refined at different temperatures by the Rietveld method using RietveldToTensor software.[1] The structure model of **2** derived from single-crystal data was used as the initial model. Pseudo-Voigt functions were used to fit the reflection profiles. The background was described by a Chebyshev polynomial function of the 21th order. Atomic coordinates, site-occupancy factors, and thermal displacement parameters were not refined. The temperature dependence of the unit cell parameters and the volume of **2** in the 20–400 °C temperature range (Figure S3) can be represented by the following linear equations:

$$a = 7.88353(21) + 0.00013264(95)t$$
$$b = 10.29749(38) – 0.0000139(17)t$$
$$c = 9.41817(87) + 0.0003589(40)t$$
$$\beta = 91.3987(20) – 0.0010985(91)t$$
$$V = 764.334(72) + 0.04145(33)t$$

6. Thermal analysis

Thermal behavior of **1** and **2** was studied on a NETZSCH STA 429 thermal analyzer over a temperature range of 40–700 °C. The polycrystalline sample (16.34 mg for **1** and 14.81 mg for **2**) was placed in a platinum crucible and subjected to heating at a rate of 10 °C/min.

7. Spectroscopy

The reflectance spectrum of **1** was measured using a Shimadzu SolidSpec-3700DUV spectrophotometer. The absorption spectrum of **2** was measured using a PerkinElmer Lambda 1050 spectrophotometer in an integrating sphere. The registration channels of the integrating sphere were normalized using $BaSO_4$ polycrystalline powder as a reference sample. Absorption (K/S) data were calculated based on the Kubelka−Munk function: $F(R) = (1 - R)^2/(2R) = K/S$, where R is the reflectance, K is the absorption, and S is the scattering.[7]

The absorption spectra in the IR range were measured using a Thermo Fisher Scientific Nicolet 6700 Fourier spectrometer by standard methods with KBr disc in the region of 400–4000 cm^{-1}. The Raman spectra of single crystals of **1** and **2** were measured using an EnSpectr R532 spectrometer equipped with a green laser (532 nm) combined with the Olympus BX43 microscope.

9. Computational details

The calculations for **1** and **2** were performed within the framework of the densityfunctional theory (DFT) as implemented in the SIESTA 5.0.1 program package.[9] The exchange-correlation potential within the Generalized Gradient Approximation (GGA) was approximated using the Perdew-Burke-Ernzerhof (PBE) parametrization. Core electrons were treated using the frozen core approximation, applying norm-

conserving Troullier-Martins pseudopotentials generated with the ATOM 3.2.2. program.[10] A real-space mesh cutoff of 350 Ry and the threshold of 10^{-4} eV were set for the self-consistent field convergence of the total electronic energy. The following were treated as valence electrons: Ag: $5s^1 4d^{10}$, B: $2s^2 2p^1$, O: $2s^2 2p^4$, and F: $2s^2 2p^5$. The integration of the Brillouin zone was performed by a 3 × 3 × 2 and 5 × 6 × 5 k-point grid sampling for density of states for **1** and **2**, respectively, and the Fermi level (E_f = 0 eV) was selected as the reference.

10. Topological analysis.

All calculations were performed using the ToposPro program package[11] Version 5.5.2.0, along with the extended ToposPro Topological Database (TTD).[12] If the obtained net had classifications according to several nomenclatures implemented in TTD, the RCSR classification was preferred.[13] The atomic adjacency matrix was constructed by the domain method.[14] A pair of *i*-th and *j*-th atoms is considered bound, either covalently or non-valently, if there is a common face of the atomic Voronoi-Dirichlet Polyhedron (VDP_{at}) between them, characterized by the solid angle Ω_{ij}. Interatomic contacts with Ω_{ij} < 1.5% of 4π steradians were omitted. To simplify anionic substructures, we used the cluster topologic representation with the subsequent standard representation of the found clusters.[15] The cluster representation was obtained by dividing all bonds in the crystal structure into intercluster and intracluster categories. The following topological criterion was applied: any intercluster bond must belong to at least one small cycle of bonds, while all intracluster bonds belong solely to large cycles.[11] Chemically, this means that intercluster bonds form relatively dense groups, while the intracluster bonds connect these groups together. If all bonds are ordered by the size N_i of the minimal cycle to which they belong, and there exists a ζ that

$$N_{\zeta+1} - N_{\zeta} > 2 \qquad (1)$$

holds, then all bonds with $i \leq \zeta$ are assumed intracluster, while other bonds with $i > \zeta$ are classified as intercluster. Next, 2-coordinated vertices (oxygen atoms) located between a pair of clusters were deleted from the net to further simplify it. Finally, the revealed clusters were pulled to their mass centers, resulting in the standard representation for the revealed clusters (Figure S4).

In both the structures, ζ = 6 was observed. Though the building blocks of the observed anionic substructures would be evident without a cluster search, the latter confirmed the correctness and non-alternative of our description, as ζ = 6 is the only possible value that satisfies Eq. 1.

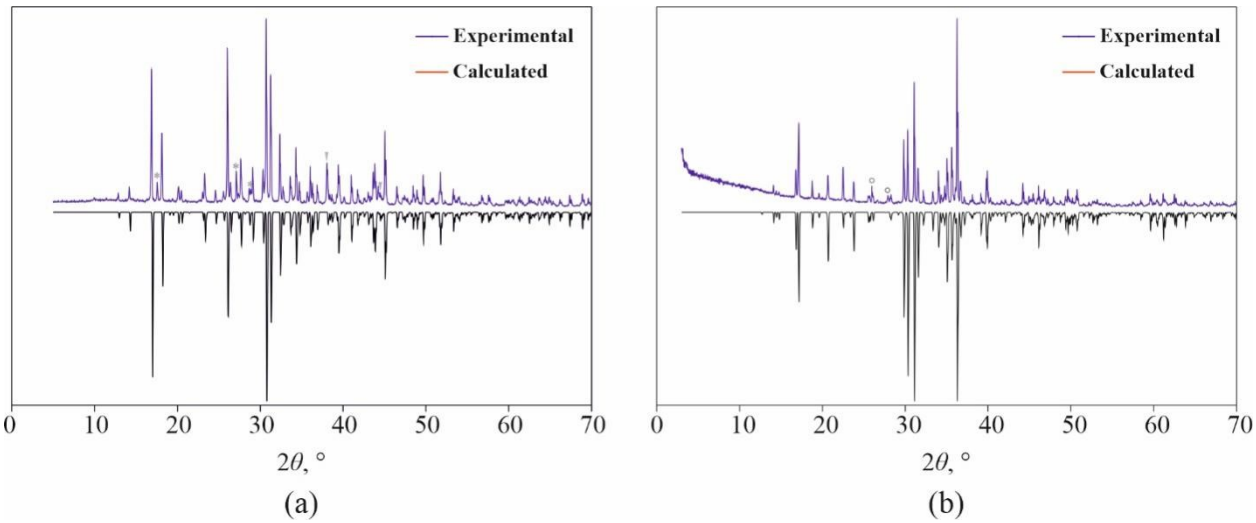

Figure S1. The experimental and simulated powder X-ray diffraction patterns of (a) **1** and (b) **2**. The asterisks and triangles in (a) show the impurity peaks of α′-$Ag_2B_8O_{13}$ and metallic silver. The circles in (b) show two unidentified impurity peaks.

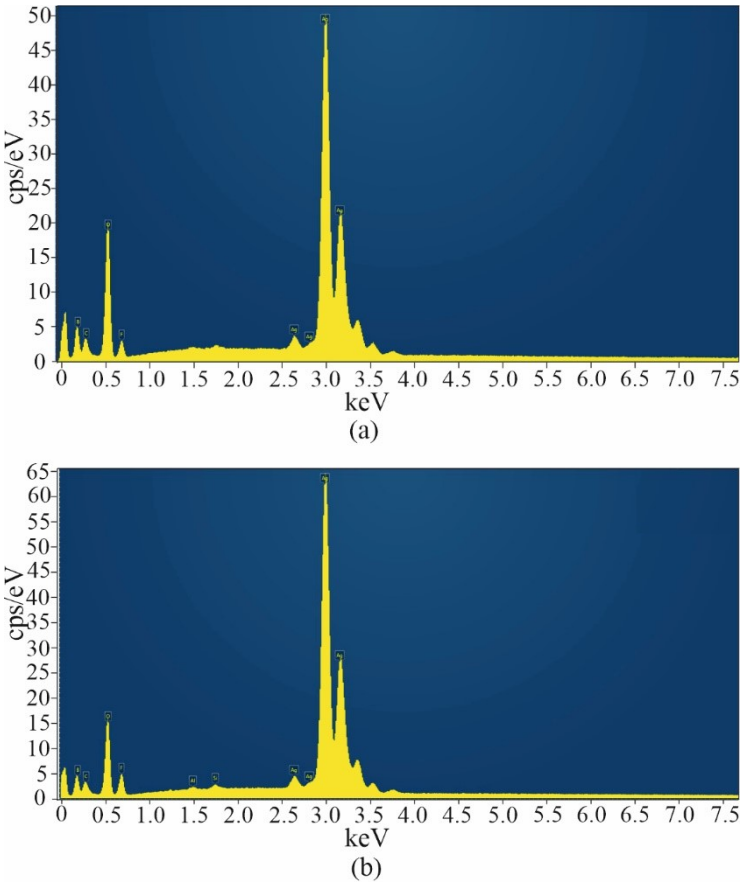

Figure S2. EDX spectra of (a) **1** and (b) **2**.

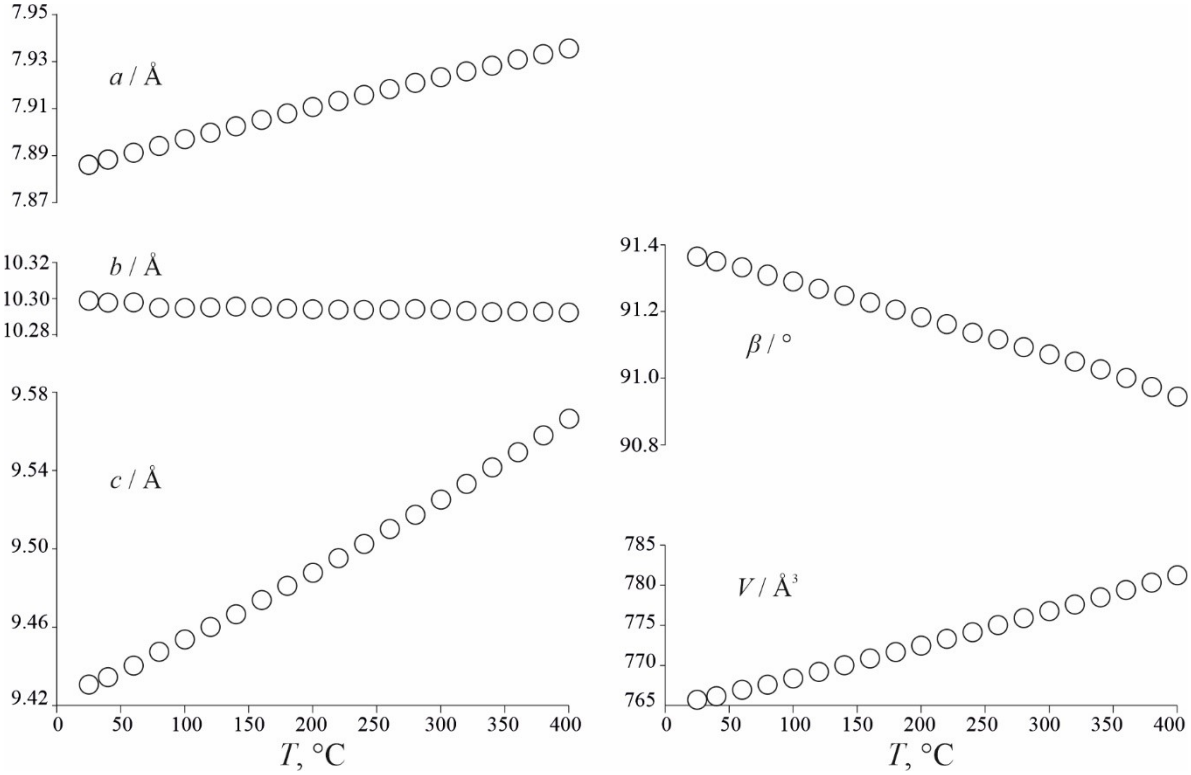

Figure S3. Temperature dependences of the unit cell parameters and volume for **2**. The uncertainties are smaller than symbols used.

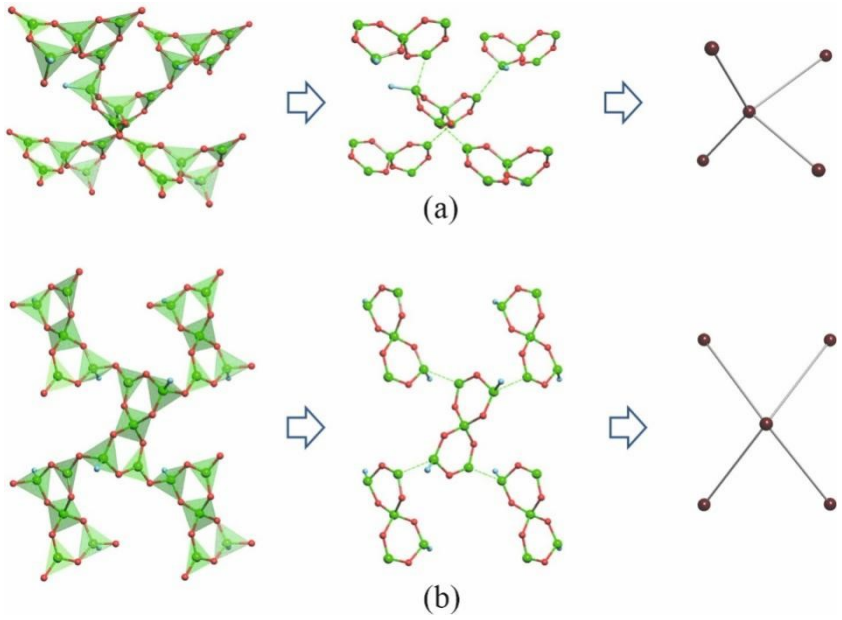

Figure S4. The cluster representation of the anionic substructure (ζ = 6) followed by the standard representations of the found clusters for **1**, viewed along the [101] direction (a) and for **2**, viewed along the [001] direction (b).

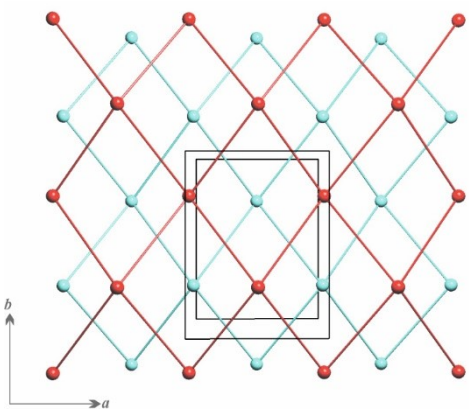

Figure S5. The underlying anionic nets of **2**. Each color designates a connectivity component.

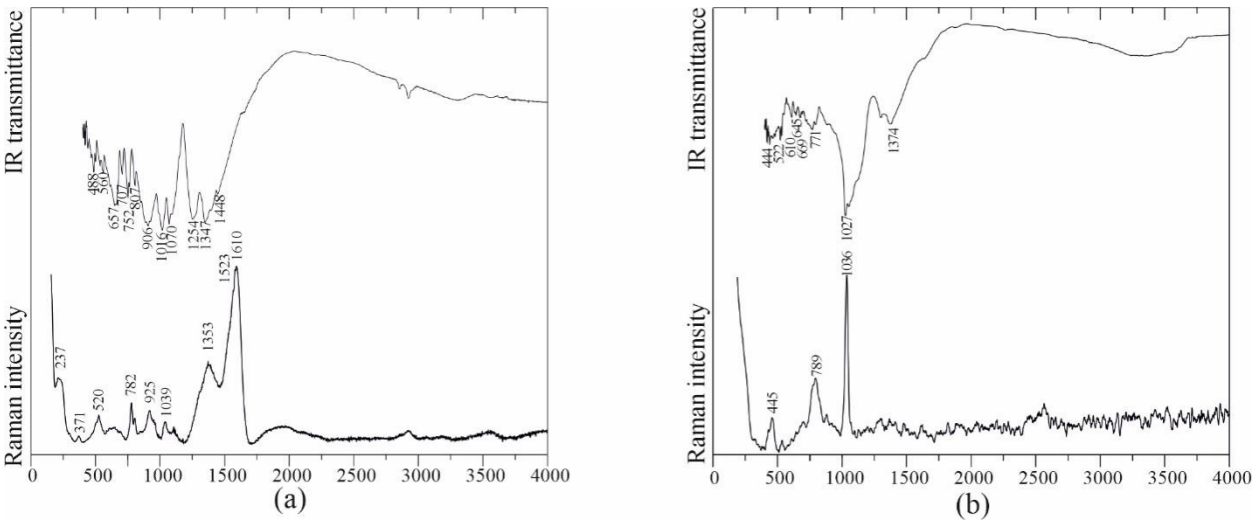

Figure S6. IR and Raman spectra of (a) **1** and (b) **2**.

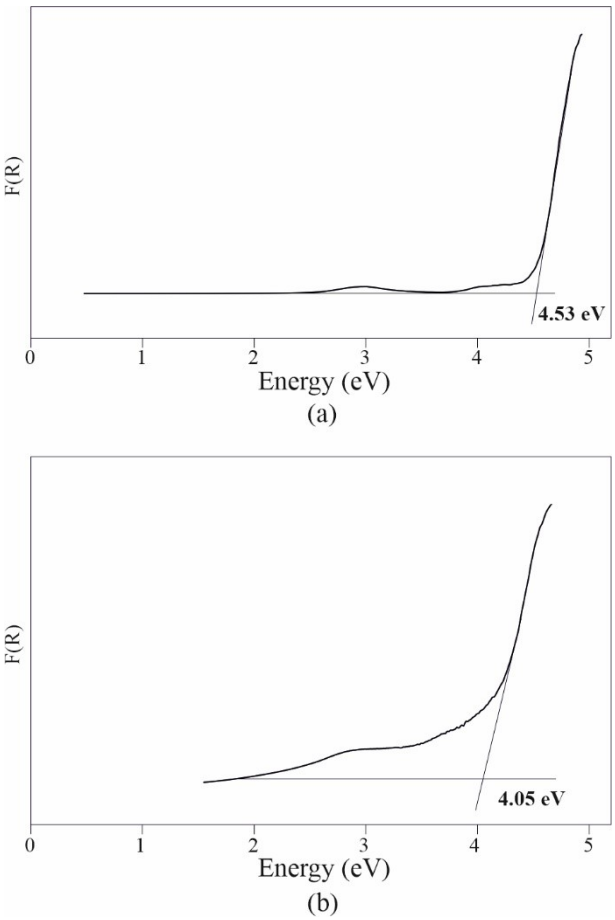

Figure S7. Absorption spectra for (a) **1** and (b) **2**.

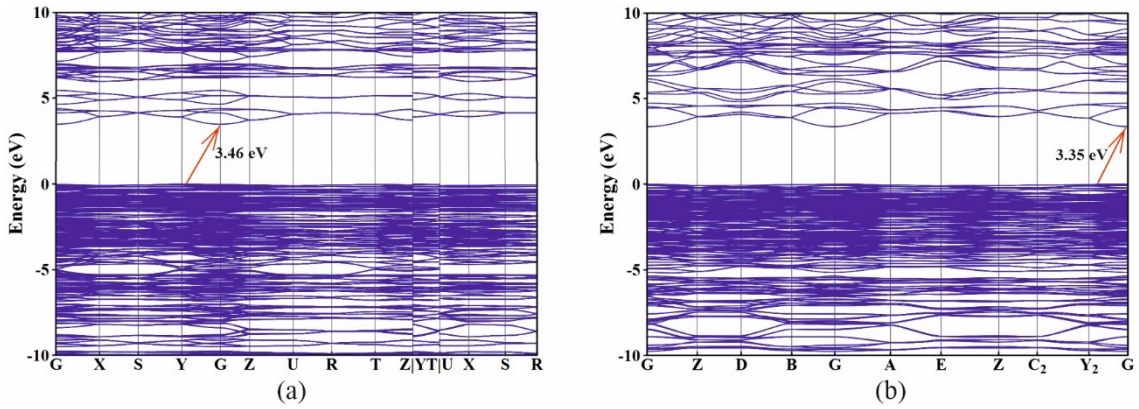

Figure S8. The band structures of (a) **1** and (b) **2** (the Fermi level is set at 0 eV).

Table S1. Crystal data and structure refinement for **1** and **2**.

Crystal data	**1**	**2**
Chemical formula	$Ag_2B_5O_8F$	$Ag_3B_5O_8F_2$
M_r	416.8	543.6
Crystal system, space group	Orthorhombic, *Pbca*	Monoclinic, $P2_1/n$
Temperature (K)	293	293
a, *b*, *c* (Å)	9.2919 (2), 13.6376 (3), 10.4234 (2)	7.8855 (2), 10.3111 (3), 9.4299 (3)
β (°)	-	91.338 (3)
V (Å^3)	1320.84 (5)	766.52 (4)
Z	8	4
Radiation type	Mo $K\alpha$	Mo $K\alpha$
μ (mm^{-1})	5.98	7.66
Crystal size (mm)	0.04 × 0.08 × 0.12	0.07 × 0.09 × 0.13
Data collection		
Diffractometer	XtaLAB Synergy, Single source at home/near, HyPix	
Absorption correction	Gaussian *CrysAlis PRO* 1.171.41.93a (Rigaku Oxford Diffraction, 2020) Numerical absorption correction based on gaussian integration over a multifaceted crystal model Empirical absorption correction using spherical harmonics, implemented in SCALE3 ABSPACK scaling algorithm.	
No. of measured, independent and observed [$I > 3\sigma(I)$] reflections	20226, 1820, 1526	11980, 1875, 1540
R_{int}	0.037	0.035
$(\sin\theta/\lambda)_{max}$ (Å^{-1})	0.724	0.725
Refinement		
$R[F^2 > 2\sigma(F^2)]$, $wR(F^2)$, S	0.017, 0.020, 1.16	0.023, 0.025, 1.24
No. of reflections	1820	1875
No. of parameters	145	163
$\Delta\rho_{max}$, $\Delta\rho_{min}$ (e Å^{-3})	0.19, – 0.33	0.36, – 0.43

Table S2. Atomic coordinates, displacement parameters (Å^2) and bond valence sums (BVS, v.u.) in the structure of **1**.

Atom	W*y*ckoff site	*x*	*y*	*z*	U_{eq}	BVS
Ag1	8*c*	0.505739(18)	0.626863(13)	0.031995(15)	0.02064(6)	0.895(1)
Ag2	8*c*	0.174981(17)	0.602308(13)	–0.023535(14)	0.01763(5)	0.951(2)
B1	8*c*	0.3446(2)	0.64280(16)	0.5029(2)	0.0095(5)	3.04(1)
B2	8*c*	0.2887(2)	0.58704(15)	0.2780(2)	0.0095(5)	3.02(1)
B3	8*c*	0.3693(2)	0.55605(15)	0.71212(19)	0.0085(5)	3.01(1)
B4	8*c*	0.4760(2)	0.70684(15)	0.3108(2)	0.0096(5)	3.02(1)
B5	8*c*	0.1976(2)	0.69125(15)	0.6913(2)	0.0086(5)	3.02(1)
O1	8*c*	0.44416(14)	0.71200(10)	0.43692(13)	0.0121(4)	2.05(1)
O2	8*c*	0.27240(14)	0.57794(10)	0.40654(13)	0.0128(4)	2.00(1)
O3	8*c*	0.42773(13)	0.58795(10)	0.59329(12)	0.0101(4)	1.94(1)
O4	8*c*	0.22711(14)	0.69909(10)	0.56382(13)	0.0119(4)	2.01(1)
O5	8*c*	0.20833(14)	0.53746(10)	0.19067(12)	0.0110(4)	1.99(1)
O6	8*c*	0.39130(13)	0.65118(10)	0.22838(12)	0.0112(4)	2.16(1)
O7	8*c*	0.27166(14)	0.62975(10)	0.77006(12)	0.0111(4)	2.02(1)
O8	8*c*	0.59012(13)	0.75243(9)	0.25386(14)	0.0112(4)	1.98(1)
F1	8*c*	0.48074(11)	0.54029(9)	0.80558(11)	0.0133(3)	0.835(4)

Table S3. Anisotropic parameters of atomic displacements in the structure of **1**.

Atom	U_{11}	U_{22}	U_{33}	U_{12}	U_{13}	U_{23}
Ag1	0.01947(10)	0.02765(11)	0.01482(10)	0.00004(6)	0.00587(6)	0.00325(6)
Ag2	0.01541(9)	0.02621(10)	0.01128(9)	0.00179(6)	0.00117(5)	0.00120(6)
B1	0.0082(10)	0.0107(9)	0.0096(9)	–0.0018(7)	–0.0004(8)	0.0020(8)
B2	0.0094(9)	0.0092(9)	0.0100(10)	–0.0014(7)	–0.0003(7)	–0.0018(7)
B3	0.0069(8)	0.0106(9)	0.0081(9)	–0.0004(7)	–0.0019(7)	–0.0007(7)
B4	0.0096(9)	0.0103(9)	0.0091(9)	–0.0004(7)	0.0002(7)	0.0012(8)
B5	0.0074(9)	0.0112(9)	0.0073(9)	0.0002(7)	–0.0016(7)	–0.0013(7)
O1	0.0136(6)	0.0135(6)	0.0092(6)	–0.0049(5)	0.0007(5)	0.0007(5)
O2	0.0130(6)	0.0162(6)	0.0091(6)	–0.0064(5)	0.0002(5)	0.0000(5)
O3	0.0079(6)	0.0126(6)	0.0099(6)	–0.0007(5)	0.0012(5)	0.0013(5)
O4	0.0106(6)	0.0187(7)	0.0065(6)	0.0042(5)	0.0004(5)	0.0013(5)
O5	0.0122(6)	0.0123(6)	0.0084(6)	–0.0034(5)	–0.0014(5)	0.0002(5)
O6	0.0105(6)	0.0155(6)	0.0076(6)	–0.0043(5)	–0.0001(5)	–0.0003(5)
O7	0.0117(6)	0.0136(7)	0.0079(6)	0.0032(5)	0.0015(5)	0.0015(5)
O8	0.0102(7)	0.0138(6)	0.0096(6)	–0.0038(5)	0.0004(5)	0.0006(5)
F1	0.0101(5)	0.0170(6)	0.0127(5)	0.0015(4)	–0.0043(4)	0.0010(4)

Table S4. Atomic coordinates, displacement parameters (Å^2) and bond valence sums (BVS, v.u.) in the structure of **2**.

Atom	W*y*ckoff site	*x*	*y*	*z*	U_{eq}	BVS
Ag1	4*e*	–0.22944(4)	0.28963(3)	0.58183(4)	0.02857(10)	1.069(4)
Ag2	4*e*	0.13638(4)	0.25140(3)	0.66546(3)	0.01914(9)	1.044(3)
Ag3	4*e*	–0.07186(4)	0.30298(3)	0.94850(4)	0.02792(10)	0.854(2)
F1	4*e*	0.2575(3)	0.4651(2)	0.5365(2)	0.0177(6)	0.866(8)
F2	4*e*	–0.2374(3)	0.0089(2)	0.5313(2)	0.0178(6)	0.855(7)
B1	4*e*	–0.2040(5)	0.0559(3)	0.3920(4)	0.0093(9)	3.05(2)
B2	4*e*	0.2141(5)	0.4183(4)	0.3985(4)	0.0119(10)	3.03(2)
B3	4*e*	0.4617(5)	0.5034(3)	0.2584(4)	0.0092(9)	3.00(2)
B4	4*e*	0.0076(4)	0.2355(3)	0.3197(4)	0.0089(9)	3.00(2)
B5	4*e*	–0.0307(5)	0.4687(4)	0.2447(4)	0.0105(10)	3.01(2)
O1	4*e*	0.3733(3)	0.4060(2)	0.3207(3)	0.0129(7)	1.94(2)
O2	4*e*	0.1394(3)	0.2894(2)	0.4140(3)	0.0123(7)	1.96(1)
O3	4*e*	–0.1316(3)	0.1839(2)	0.4020(3)	0.0124(7)	2.08(1)
O4	4*e*	0.0754(3)	0.1329(2)	0.2277(2)	0.0106(6)	2.09(1)
O5	4*e*	–0.0981(3)	–0.0342(2)	0.3203(3)	0.0125(7)	2.16(2)
O6	4*e*	–0.0611(3)	0.3397(2)	0.2204(2)	0.0125(7)	1.94(1)
O7	4*e*	–0.1236(3)	0.5658(2)	0.1781(3)	0.0123(7)	2.12(1)
O8	4*e*	0.0974(3)	0.5097(2)	0.3320(3)	0.0125(6)	2.04(2)

Table S5. Anisotropic parameters of atomic displacements in the structure of **2**.

Atom	U_{11}	U_{22}	U_{33}	U_{12}	U_{13}	U_{23}
Ag1	0.03393(19)	0.01949(15)	0.0332(2)	–0.00531(11)	0.02083(14)	–0.01376(12)
Ag2	0.02802(16)	0.01029(13)	0.01912(15)	–0.00103(10)	0.00107(11)	–0.00008(10)
Ag3	0.02317(17)	0.02248(16)	0.0385(2)	–0.01026(11)	0.00840(14)	–0.00522(12)
B1	0.0080(17)	0.0085(16)	0.0113(17)	0.0005(11)	0.0012(13)	–0.0007(13)
B2	0.0133(18)	0.0108(16)	0.0115(17)	–0.0014(13)	–0.0004(13)	–0.0043(13)
B3	0.0104(17)	0.0062(16)	0.0111(16)	–0.0004(12)	0.0003(13)	0.0043(12)
B4	0.0063(16)	0.0057(15)	0.0147(18)	–0.0015(11)	–0.0007(13)	0.0001(13)
B5	0.0090(17)	0.0124(17)	0.0101(17)	–0.0020(12)	0.0018(13)	–0.0016(12)
O1	0.0112(12)	0.0114(11)	0.0162(12)	0.0007(8)	0.0026(9)	0.0050(9)
O2	0.0104(12)	0.0119(11)	0.0144(12)	–0.0028(8)	–0.0033(9)	0.0033(9)
O3	0.0111(11)	0.0078(11)	0.0186(12)	–0.0040(8)	0.0065(9)	–0.0046(9)

O4	0.0142(12)	0.0064(10)	0.0114(11)	–0.0007(8)	0.0051(9)	0.0003(8)
O5	0.0118(11)	0.0088(11)	0.0170(12)	0.0005(8)	0.0047(9)	–0.0020(9)
O6	0.0166(12)	0.0072(11)	0.0136(12)	0.0012(8)	–0.0059(9)	0.0022(9)
O7	0.0081(11)	0.0102(11)	0.0185(12)	0.0003(8)	–0.0002(9)	0.0021(9)
O8	0.0101(11)	0.0094(11)	0.0179(12)	–0.0014(8)	–0.0035(9)	–0.0028(9)
F1	0.0226(11)	0.0199(10)	0.0103(9)	–0.0054(8)	–0.0037(8)	–0.0023(8)
F2	0.0190(11)	0.0228(10)	0.0117(9)	–0.0048(8)	0.0034(8)	0.0032(8)

Table S6. Selected bond lengths (Å) in the structure of **1**.

Bond	Length	Bond	Lenght
Ag1—O1^{i}	2.4776 (14)	B2—O2	1.354 (2)
Ag1—O2^{ii}	2.6448 (13)	B2—O5	1.358 (2)
Ag1—O4^{ii}	2.4897 (13)	B2—O6	1.393 (2)
Ag1—O6	2.3304 (13)	B3—O3	1.421 (2)
Ag1—F1^{iii}	2.6490 (11)	B3—O5^{vii}	1.482 (2)
Ag1—F1^{iv}	2.8423 (12)	B3—O7	1.483 (2)
Ag2—O1^{v}	2.7664 (13)	B3—F1	1.438 (2)
Ag2—O2^{vi}	2.6102 (14)	B4—O1	1.349 (2)
Ag2—O3^{v}	2.4177 (12)	B4—O6	1.391 (2)
Ag2—O4^{i}	2.8982 (14)	B4—O8	1.365 (2)
Ag2—O5	2.4214 (13)	B5—O4	1.361 (2)
Ag2—O7^{iii}	2.3613 (13)	B5—O7	1.360 (2)
B1—O1	1.490 (2)	B5—O8^{viii}	1.384 (2)
B1—O2	1.497 (2)		
B1—O3	1.430 (2)		
B1—O4	1.478 (2)		

Symmetry code(s): (i) *x*, –*y*+3/2, *z*–1/2; (ii) *x*+1/2, *y*, –*z*+1/2; (iii) *x*, *y*, *z*–1; (iv) –*x*+1, –*y*+1, –*z*+1; (v) *x*–1/2, *y*, –*z*+1/2; (vi) –*x*+1/2, –*y*+1, *z*–1/2; (vii) –*x*+1/2, –*y*+1, *z*+1/2; (viii) *x*–1/2, –*y*+3/2, –*z*+1.

Table S7. Selected bond lengths (Å) in the structure of **2**.

Bond	Length	Bond	Lenght
Ag1—O3	2.173 (3)	B1—O3	1.440 (4)
Ag1—O4^{i}	2.236 (2)	B1—O5	1.430 (4)
Ag1—O8^{ii}	2.446 (2)	B1—O7^{vii}	1.502 (4)
Ag1—F1^{ii}	2.771 (2)	B1—F2	1.430 (4)
Ag1—F2	2.934 (2)	B2—O1	1.474 (4)
Ag2—O2	2.404 (3)	B2—O2	1.462 (4)
Ag2—O3^{iii}	2.928 (2)	B2—O8	1.450 (4)
Ag2—O5^{iv}	2.264 (2)	B2—F1	1.422 (4)
Ag2—O6^{iii}	2.605 (2)	B3—O1	1.364 (4)
Ag2—O7^{ii}	2.397 (2)	B3—O4^{viii}	1.373 (4)
Ag2—F1	2.702 (2)	B3—O5^{viii}	1.377 (4)
Ag2—F2^{iv}	3.369 (2)	B4—O2	1.462 (4)
Ag3—O1^{i}	2.501 (2)	B4—O3	1.459 (4)
Ag3—O2^{i}	2.482 (2)	B4—O4	1.477 (4)
Ag3—O6^{v}	2.591 (2)	B4—O6	1.517 (4)
Ag3—O7^{ii}	2.391 (2)	B5—O6	1.370 (4)
Ag3—F1^{i}	3.192 (2)	B5—O7	1.383 (4)
Ag3—F2^{vi}	2.611 (2)	B5—O8	1.356 (4)
Ag3—F2^{iii}	3.351 (2)		

Symmetry code(s): (i) *x*–1/2, –*y*+1/2, *z*+1/2; (ii) –*x*, –*y*+1, –*z*+1; (iii) *x*+1/2, –*y*+1/2, *z*+1/2; (iv) –*x*, –*y*, –*z*+1; (v) *x*, *y*, *z*+1; (vi) –*x*–1/2, *y*+1/2, –*z*+3/2; (vii) –*x*–1/2, *y*–1/2, –*z*+1/2; (viii) –*x*+1/2, *y*+1/2, –*z*+1/2.

Table S8. Assignment of the vibrational bonds observed in the Raman and infrared spectra for **1**.

Raman peaks, cm^{-1}	IR peaks, cm^{-1}	Assignment
1610		
1523		asymmetric stretching vibrations of $[BO_3]F$[15]
	1448	asymmetric stretching of the vibrations $[BO_3]$ groups
1347	1347	asymmetric stretching of the vibrations $[BO_3]$ groups
	1254	asymmetric stretching of the vibrations B–F
	1070	asymmetric stretching vibrations $[BO_4]F$
1039	1016	asymmetric stretching vibrations $[BO_4]F$
925	906	symmetric stretching vibrations $[BO_3]$
	807	out-of-plane symmetric stretching of the $[BO_3F]$
782	762	symmetric stretching vibrations $[BO_3F]$
	752	out-of-plane bending vibrations $[BO_3]$ groups
	707	out-of-plane bending vibrations $[BO_3]$ groups
	657	out-of-plane bending vibrations $[BO_3]$ groups
	560	In-plane bending vibrations $[BO_3]$ groups
520	535	In-plane bending vibrations $[BO_3F]$ groups[16]
	501	In-plane bending vibrations $[BO_3]$ groups[15,17]
	488	In-plane bending vibrations $[BO_3]$ groups[15,17]
	468	In-plane bending vibrations $[BO_3]$ groups[15,17]
	440	In-plane bending vibrations $[BO_3]$ groups[15,17]

Table S9. Assignment of the vibrational bonds observed in the Raman and infrared spectra for **2**.

Raman peaks, cm^{-1}	IR peaks, cm^{-1}	Assignment
	1374	asymmetric stretching vibrations $[BO_3]$ groups
1036	1027	Asymmetric stretching vibrations of $[BO_3F]$ groups[17]
789	771	symmetric stretching vibrations $[BO_3F]$
	669	out-of-plane bending of the $[BO_3]$ groups
	645	In-plane bending vibrations $[BO_3]$ groups[17]
	610	In-plane bending vibrations $[BO_3]$ groups[16]
	522	In-plane bending vibrations $[BO_3F]$ groups[16]
445	444	In-plane bending vibrations $[BO_3]$ groups[15]

Table S10. Some characteristics of the anionic net represented by bifluoropentaborate clusters with different configurations of stereocenters.

Compound	Chirality of the crystal	Bifluorinated pentaborate stereoisomer	Chirality of the anionic net	Dimensionality of the anionic net	Type of the anionic net
$Rb_3B_5O_8F_2$	yes	*S*,*R*,*R*- or *R*,*S*,*S*-	yes	2D	**sql**
$K_{0.6}Rb_{2.4}B_5O_8F_2$					
$LiNa_{0.9}K_{0.1}B_5O_8F_2$	no	*R*,*R*,*R*- and *S*,*S*,*S*-	yes		
$Ag_3B_5O_8F_2$					

References

1 R. S. Bubnova, V. A. Firsova, S. N. Volkov and S. K. Filatov, *Phys. Chem. Glas.*, **2018**, *44*, 33–40.

2 Rigaku Oxford Diffraction, CrysAlisPRO Software System, Version 1.171.41.104a (2021), Rigaku Corporation, Oxford, UK.

3 L. Palatinus and G. Chapuis, *J. Appl. Crystallogr.*, **2007**, *40*, 786–790.

4 V. Petříček, L. Palatinus, J. Plášil and M. Dušek, *Z. Kristallogr. Cryst. Mater.*, **2023**, *238*, 271–282.

5 K. Momma and F. Izumi, *J. Appl. Crystallogr.*, **2008**, *41*, 653–658.

6 Dowty, E. ATOMS for Windows; Version 6.1; Shape Software: Kingsport, TN, USA, 2000.

7 P. Kubelka and F. Z. Munk, *Technol. Phys.*, **1931**, *12*, 593–601.

8 L. L. Cao, G. Peng, W. B. Liao, T. Yan, X. F. Long and N. Ye, *CrystEngComm*, **2020**, *22*, 1956−1961.

9 J. M. Soler, E. Artacho, J. D. Gale, A. García, J. Junquera, P. Ordejón and D. Sánchez-Portal, *J. · Phys.: Condens. Matter.*, **2002**, *14*, 2745–2779.

10 N. Troullier and J. L. Martins, *Phys. Rev. B*, **1991**, *43*, 1993–2006.

11 V. A. Blatov, A. P. Shevchenko and D. M. Proserpio, *Cryst. Growth. Des.*, **2014**, *14*, 3576–3586.

12 E. V. Alexandrov, A. P. Shevchenko and V. A. Blatov, *Cryst. Growth. Des.*, **2019**, *19*, 2604–2614.

13 M. O'Keeffe, M. A. Peskov, S. J. Ramsden and O. M. Yaghi, *Acc. Chem. Res.*, **2008**, *41*, 1782–1789.

14 V. A. Blatov, A. P. Shevchenko and V. N. Serenzhkin, *Acta Crystallogr. A*, **1995**, *51*, 909–916.

15 A. P. Shevchenko and V. A. Blatov, *Struct. Chem.*, **2021**, *32*, 507–519.

16 Z. Chen, Z. Li, D. Chu, F. Zhang, X. Li, Z. Yang, X. Long and S. Pan, *Chem. Commun.*, **2022**, *58*, 12369–12372.

17 Z. Lu, F. Zhang, A. Tudi, Z. Yang and S. Pan, *Chem. Commun.*, **2020**, *56*, 15333–15336.

18 T. Baiheti, A. Tudi, M. Gai, X. Wang and S. Han, *Inorg. Chem.*, **2023**, *62*, 5008–5015.